ACS OMEGA

Open Access

http://pubs.acs.org/journal/acsodf

Article

Production Characteristics of Volatiles from Anthracite Cracking via Microwave-Induced Discharge

Lei Zhang, Mingjun Liu, Minghong Han, Yang Yu, Wei Zhou, Jihui Gao, Yanlin Su, Junfeng Li, Pengxiang Wang,* and Guangbo Zhao

Cite This: *ACS Omega* 2024, 9, 8947−8953

Read Online

ACCESS | Metrics & More | Article Recommendations | Supporting Information

ABSTRACT: The ignition of anthracite with arc plasma has not been applied due to its low chemical effect and volatile content in anthracite. The nonequilibrium plasma generated by a microwave-induced discharge has the ability to break branch chains and aromatic ring structures by kinetic effects, which has the potential for anthracite cracking and ignition. This work investigated anthracite cracking by microwave-induced discharges under an Ar/N_2 atmosphere. Results showed that the maximum levels of CO production, total gas production, and total gas generation rate occur in 20% argon content due to an increase in the number of electrons and a decrease in the total electronic states excitation rate constant with an increase in the argon content. The total gas production in plasma cracking is larger than that by pyrolysis, indicating the crack of polycyclic aromatic hydrocarbon by plasma. In addition, we attempted anthracite combustion under an 80% N_2 and 20% O_2 atmosphere.

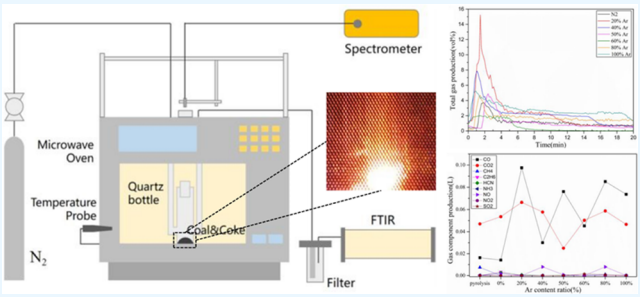

1. INTRODUCTION

Some new advanced ignition technologies have been developed in recent years in thermal power plants for saving oil and stabling flame.[1] Among these technologies, plasma-assisted ignition has great potential for coal combustion. However, its application still has difficulties with regard to high-rank coal due to its low reactivity[2] and volatile content.[3] Most of the current plasma ignition technology is based on arc plasma,[4] which is a type of equilibrium plasma. Equilibrium plasma has a strong thermal effect but weak kinetic effect, while most of the nonequilibrium plasma such as corona,[5] dielectric barrier discharge,[6] and microwave discharge[7] have excellent kinetic effects due to their high electron temperatures.[8]

Microwave-induced discharge is a type of nonequilibrium plasma triggered by metal and dielectric materials under microwave irradiation below the breakdown threshold.[9] It has been applied in many areas, such as biomass gasification,[10,11] chip etching,[12] and volatile organic compound processing.[13] Microwave-induced discharge shows the ability to break the chain and aromatic ring structure when applied for cracking cyclic organic compounds such as toluene,[14] cyclohexane, xylene, and ethylbenzene.[15] Therefore, it has the potential for cracking the carbon skeleton of coal. In our previous work, we observed a centimeter-scale plasma produced by microwave-induced discharge, which can upgrade the air ionization and expand the range of a flame.[16,17] However, the enhancing effect of microwave-induced discharge on anthracite cracking is still unclear. Moreover, the addition of other working gases, such as Ar, H_2O, and He, can regulate the energy transfer pathway in plasma,[18−20] leading to changes in production components. So far, the influence of the atmosphere on the cracking of anthracite by microwave-induced discharge is not clear.

This work investigated anthracite cracking by microwave-induced discharge and its effects on gas production by argon contents in this process. To reveal the kinetic effects of microwave-induced discharge, we detected the spectrum of plasma to identify excited-state molecules. This work also attempted to assess anthracite combustion assisted by microwave-induced discharge under the conditions of 80% N_2 and 20% O_2 atmosphere to study the possibility of high-rank coal ignition by microwave-induced discharge.

2. EXPERIMENTS AND CALCULATION

2.1. Experiments. In this work, the cracking and ignition of anthracite by microwave-induced discharge was conducted, while the pyrolysis of anthracite was carried out as the control group. The mass of coke and coal is 1 g. The sizes of coal and coke range from 0.150 to 0.178 mm and 0.425 to 0.850 mm, respectively. The proximate and elemental analyses are shown

Received: September 14, 2023
Revised: December 21, 2023
Accepted: December 27, 2023
Published: February 15, 2024

https://doi.org/10.1021/acsomega.3c05977
ACS Omega 2024, 9, 8947−8953

Table 1. Proximate Analysis and Elemental Analysis of Coal and Coke

	proximate analysis (wt %)				elemental analysis (wt %)				
sample	M_{ar}	A_{ar}	V_{ar}	FC_{ar}	C_{daf}	H_{daf}	O_{daf}	N_{daf}	S_{daf}
coal	3.63	13.05	5.99	77.33	91.62	3.11	3.75[a]	1.46	0.07
coke	5.35	18.39	4.06	72.21	83.62	0.98	14.32[a]	1.02	0.06

[a]The result is attained by the subtraction method.

in Table 1. The proximate analyses were determined according to the Chinese National Standard GB/T 212−2008, while the ultimate analyses were determined according to the Chinese National Standard GB/T 476−2008 (carbon and hydrogen), GB/T 19227−2008 (nitrogen), and GB/T 214−2007 (sulfur).[21] The total gaseous flow was 0.5 L/min in all cases.

In pyrolysis experiments, coke and coal were placed in a tube furnace, heated from 25 to 900 °C at 10 °C/min, and retained for 2 h under a nitrogen atmosphere. Micrographs of the coal and coke particles were measured by scanning electron microscopy (SEM, JSM-7401F), as shown in Figure S1. The gas produced during pyrolysis was cooled and filtered to remove the tar before component analysis.

In the cracking and combustion experiments, coal and coke within a quartz reactor were placed in a microwave oven. The argon contents of the atmosphere in cracking experiments were set as 0, 20, 40, 50, 60, 80, and 100%, while the atmosphere of combustion experiments constituted 80% N_2 and 20% O_2. The microwave power was 800 W and the running time of each case was 20 min. The plasma was generated by a microwave-induced discharge between cokes. Without coke and coal, microwaves cannot directly induce discharge in the reactor. The spectrum of plasma during cracking was detected by a spectrometer through an observation hole on the top of the microwave oven. The method and process of gas component analysis were set to be consistent with the pyrolysis experiments.

The tube furnace used in pyrolysis experiments was a GSL-1100X. The microwave oven used in cracking experiments was an MAS-II operator, and its frequency value was up to 2.45 GHz, as shown in Figure 1. A plasma spectrum detector (Avaspec-ULS4096CL-EVO) was used to detect excited-state molecules created by discharge. Its integral time was set to 50 ms, and the measurement range of wavelength was 200−1100 nm. A Fourier transform infrared spectrometer (FTIR, DX-4000) was used to analyze gaseous production in cracking and pyrolysis experiments. CO, CO_2, H_2O, HCN, NH_3, NO, NO_2, and SO_2 were detected in each experiment. Because of the drying and filtering of gas products, the data on H_2O do not reflect the real contents of H_2O in gas products.

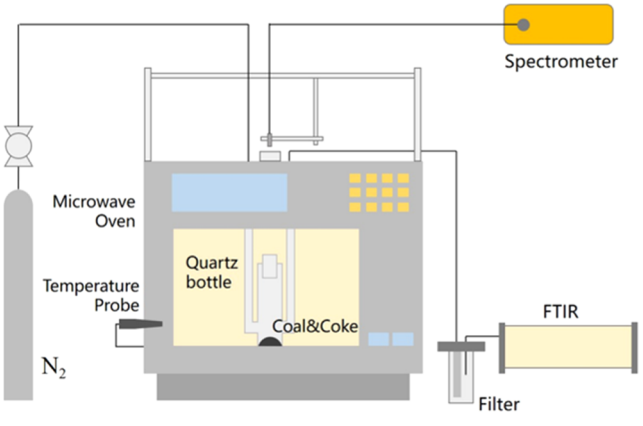

Figure 1. Microwave-induced discharge system.

2.2. Calculation. To reveal the mechanisms of this phenomenon, we calculated the reaction rate constant and electron energy transferred in the electron impact reactions with different argon contents. The reactions considered in the nitrogen and argon discharge are shown in Table 2. The cross sections of electron impact reactions were obtained from lxcat.

Table 2. List of Reactions and Rate Constants

reaction		energy (eV)	references
$e + Ar \rightarrow e + Ar$	(1)	0	a
$e + Ar \rightarrow e + Ar(4s)$	(2)	11.55	a
$e + Ar \rightarrow e + Ar(4p)$	(3)	13.00	a
$e + Ar \rightarrow e + Ar(4d)$	(4)	14.00	a
$e + Ar \rightarrow 2e + Ar^+$	(5)	15.70	a
$e + N_2 \rightarrow e + N_2$	(6)	0	b
$e + N_2 \rightarrow e + N_2(rot)$	(7)	0.02	b
$e + N_2 \rightarrow e + N_2(v = 1)$	(8)	0.29	b
$e + N_2 \rightarrow e + N_2(v = 2)$	(9)	0.59	b
$e + N_2 \rightarrow e + N_2(v = 3)$	(10)	0.88	b
$e + N_2 \rightarrow e + N_2(v = 4)$	(11)	1.17	b
$e + N_2 \rightarrow e + N_2(v = 5)$	(12)	1.47	b
$e + N_2 \rightarrow e + N_2(v = 6)$	(13)	1.76	b
$e + N_2 \rightarrow e + N_2(v = 7)$	(14)	2.06	b
$e + N_2 \rightarrow e + N_2(v = 8)$	(15)	2.35	b
$e + N_2 \rightarrow e + N_2(A^3)$	(16)	6.17	b
$e + N_2 \rightarrow e + N_2(B^3)$	(17)	7.35	b
$e + N_2 \rightarrow e + N_2(W^3)$	(18)	7.36	b
$e + N_2 \rightarrow e + N_2(B'^3)$	(19)	8.16	b
$e + N_2 \rightarrow e + N_2(a'^1)$	(20)	8.40	b
$e + N_2 \rightarrow e + N_2(a^1)$	(21)	8.55	b
$e + N_2 \rightarrow e + N_2(w^1)$	(22)	8.89	b
$e + N_2 \rightarrow e + 2N$	(23)	9.75	c
$e + N_2 \rightarrow e + N_2(C^3)$	(24)	11.03	b
$e + N_2 \rightarrow e + N_2(E^3)$	(25)	11.87	b
$e + N_2 \rightarrow e + N_2(a''^1)$	(26)	12.25	b
$e + N_2 \rightarrow e + N_2(sum)$	(27)	13.00	b
$e + N_2 \rightarrow 2e + N_2^+$	(28)	15.60	b

[a]Biagi-v7.1 database, www.lxcat.net, retrieved on May 27, 2022. [b]SIGLO database, www.lxcat.net, retrieved on May 27, 2022. [c]Itikawa database, www.lxcat.net, retrieved on May 27, 2022.

https://doi.org/10.1021/acsomega.3c05977
ACS Omega 2024, 9, 8947−8953

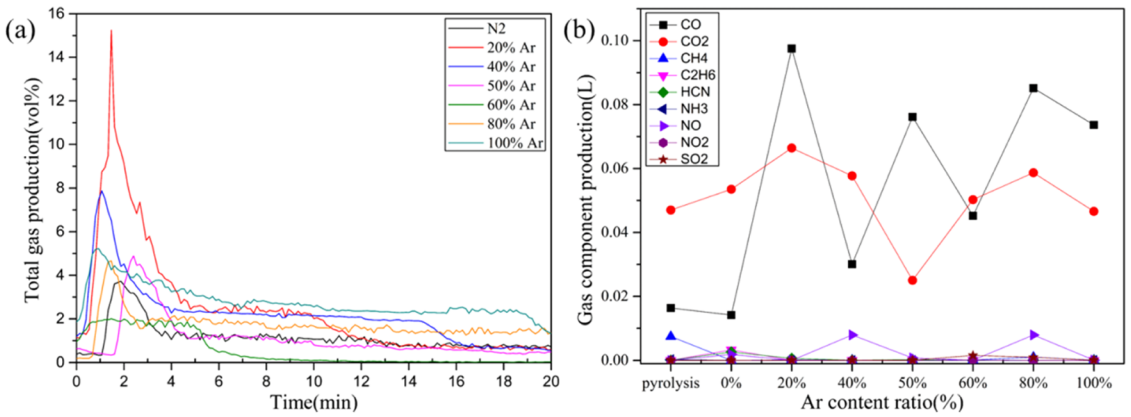

Figure 2. (a) Total gaseous production on different ratios of Ar/N_2. (b) Gas component production in different ratios of Ar/N_2.

Table 3. Gas Component Production under Different Conditions

gas (L)	pyrolysis	N_2	20%Ar	40%Ar	50%Ar	60%Ar	80%Ar	100%Ar
CO	0.01636	0.01417	0.09753	0.03007	0.07615	0.0452	0.08514	0.07365
CO_2	0.04702	0.05350	0.06640	0.05771	0.02501	0.05026	0.05866	0.04659
CH_4	7.430×10^{-3}	1.347×10^{-7}	2.128×10^{-4}	1.021×10^{-4}	1.870×10^{-4}	1.358×10^{-4}	1.028×10^{-3}	9.638×10^{-5}
C_2H_6	4.709×10^{-5}	3.281×10^{-3}	2.965×10^{-5}	2.399×10^{-5}	3.321×10^{-5}	8.742×10^{-5}	2.472×10^{-5}	3.001×10^{-5}
HCN	7.100×10^{-5}	2.624×10^{-3}	6.294×10^{-4}	6.166×10^{-5}	2.520×10^{-4}	4.646×10^{-5}	6.317×10^{-5}	4.737×10^{-5}
NH_3	2.445×10^{-4}	8.647×10^{-5}	2.128×10^{-6}	2.446×10^{-6}	3.624×10^{-6}	8.722×10^{-5}	3.561×10^{-6}	3.543×10^{-6}
NO	0	1.858×10^{-3}	2.940×10^{-7}	7.920×10^{-3}	7.408×10^{-4}	7.237×10^{-5}	7.920×10^{-3}	1.111×10^{-4}
NO_2	0	5.275×10^{-6}	0	0	0	1.636×10^{-4}	0	0
SO_2	7.764×10^{-6}	3.132×10^{-5}	9.845×10^{-5}	9.775×10^{-5}	6.852×10^{-5}	1.553×10^{-3}	9.858×10^{-4}	8.442×10^{-5}
total	0.0711	0.1030	0.1650	0.0960	0.1020	0.0970	0.1540	0.1210

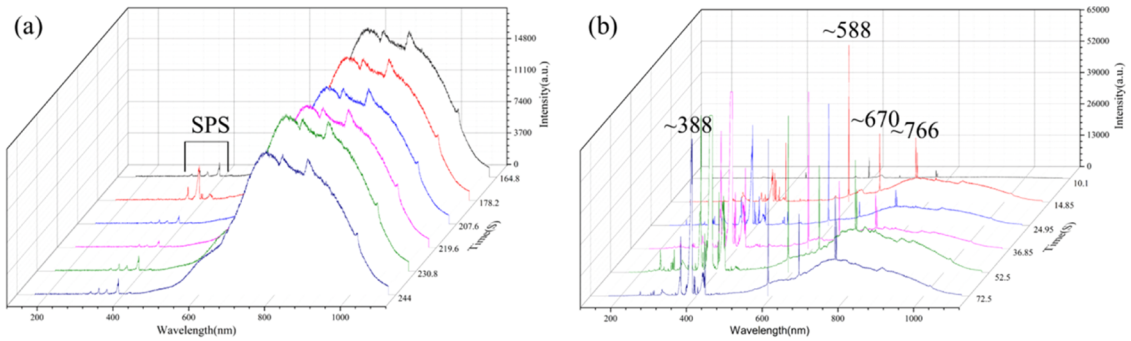

Figure 3. Spectrum of microwave-induced coke discharge in (a) pure N_2 and (b) pure Ar.

The data of cross sections used in this study are also provided in the Supporting Information. The reaction rate constants of electron impact reactions are calculated from the electron energy distribution function (EEDF) by BOLSIG+,[22] which computes the Boltzmann transport equation by providing cross sections of electron impact reactions. The conditions of numerical simulation are set as follows: temperature, 300 K; range of electron energy, 0.1−20 eV; and interval, 0.1 eV.

3. RESULTS

Figure 2a shows that the maximum total gas generation rate is above 15 vol % for discharge in 20% argon. The peak in 50% argon content was the last to appear (149s), while the time of peak for pure nitrogen appeared earliest (57s). In pyrolysis, gas production continued for several hours. This means that the generation rate of total gas production by microwave plasma cracking is higher than that by pyrolysis.

Gas component productions of pyrolysis and microwave plasma cracking are shown in Figure 2b and Table 3. CO and CO_2 are the main gaseous products in plasma cracking and pyrolysis, while the productions of CH_4, C_2H_6, HCN, NH_3, NO, NO_2, and SO_2 are low. Compared with pyrolysis and cracking in pure nitrogen, the amount of CO generated increases as argon is added to the atmosphere. CO is a type of combustible gas, and the highest level of CO generated is 0.0975 L in 20% argon. The amount of CH_4 generated in plasma cracking is lower than that by pyrolysis. In detail, compared with discharge in pure nitrogen, the production of methane is higher for the discharge in a mixture of argon and nitrogen. In the conditions of microwave-induced discharge, the production of C_2H_6 and HCN in pure nitrogen is more than that by pyrolysis and with the addition of argon. The production of NO, NO_2, and SO_2 for microwave plasma cracking increased, while NH_3 production decreased compared with that of pyrolysis. As shown in Table 3, compared with

https://doi.org/10.1021/acsomega.3c05977
ACS Omega 2024, 9, 8947−8953

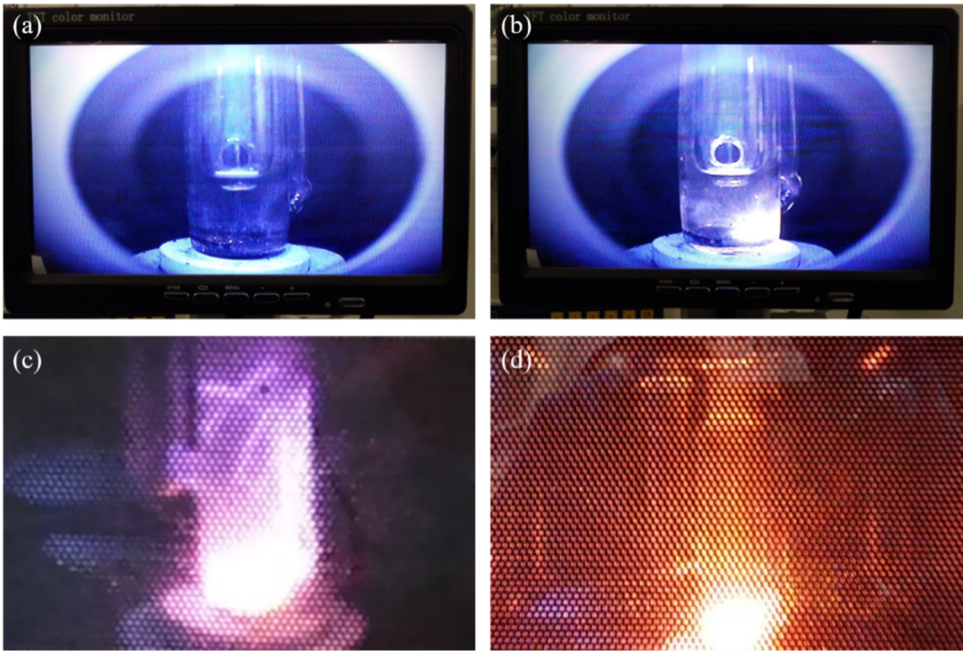

Figure 4. (a) Spark-like discharge and (b) arc-like discharge in microwave-induced discharge in nitrogen. (c) Filamentous-like discharge in argon and (d) combustion with microwave-induced discharge in 20% O_2 and 80% N_2.

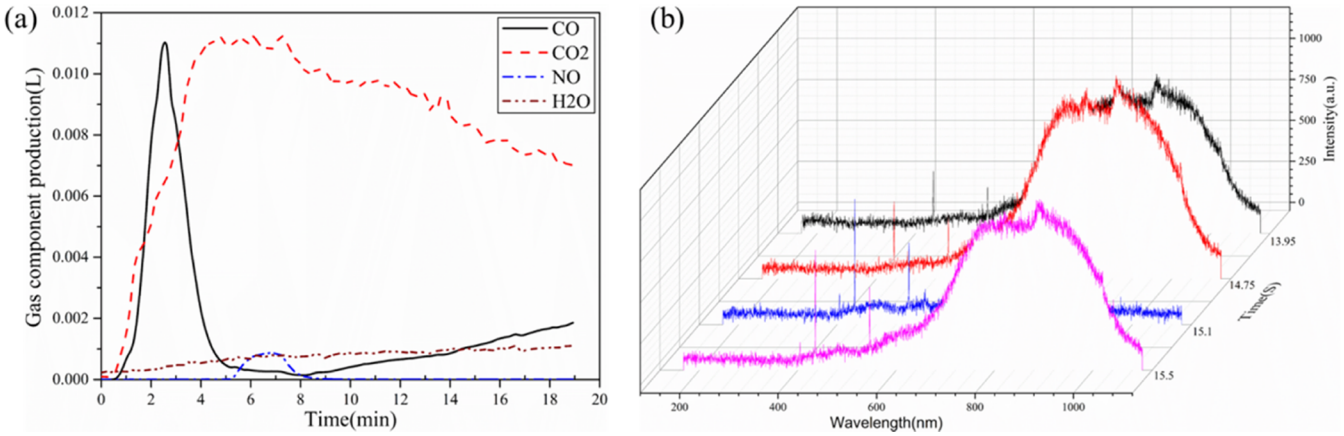

Figure 5. (a) Main gaseous component production and (b) plasma spectrum in the microwave ignition experiment under 80% N_2 and 20% O_2.

pyrolysis, the higher production of element C in the microwave-induced discharge crack indicates the breaking of polyaromatic hydrogen by microwave plasma.

The plasma spectra in microwave-induced discharge under pure nitrogen and argon are shown in Figure 3. The discharge was hardly triggered in coals without coke affected by the microwave. In nitrogen discharge, the SPS lines of N_2(357.45−402.51 nm) were detected, as shown in Figure 3a, which originated from the de-excitation of $N_2(C)$ to $N_2(A)$ and $N_2(B)$.[23] For discharge in argon, the de-excitation lines at 200−450, 588, 670, and 766 nm were detected, as shown in Figure 3b. The latter three may originate from the de-excitation of Ar(4d → 4p) and Ar(4p → 4s). The existence of excited-state nitrogen and argon demonstrates kinetic effects on anthracite cracking by microwave-induced discharge. Moreover, plasma transitions were observed in the microwave-induced discharge process. In nitrogen, the plasma transition from the spark-like discharge to arc-like discharge occurred at around 2 min, as shown in Figure 4a,b, while the plasma transition from spark-like discharge to filamentous-like discharge occurred at around 10 min in argon, as Figure 4c.

Figure 5a shows the gas component production under an 80% N_2 and 20% O_2 atmosphere. The amount of CO increases sharply at the beginning of the experiment, and the peak appears at 145s. After that, the CO content decreases to nearly zero after 6 min and then increases linearly. The amount of CO_2 production reaches the maximum level at 255s and decreases after that. The generation of NO under the conditions of combustion demonstrates that combustion in this period is drastic. The production of NH_3, HCN, C_2H_6, and CH_4 is close to zero. Moreover, the image of combustion is shown in Figure 4d.

The N_2 SPS lines and de-excitation lines in the ranges of 430−440 and 595−605 nm were detected, as shown in Figure 5b. The last one may originate from $O_2(b \rightarrow a)$.[23] The de-excitation lines show the kinetic effects of combustion by microwave-induced discharge.

https://doi.org/10.1021/acsomega.3c05977
ACS Omega 2024, 9, 8947−8953

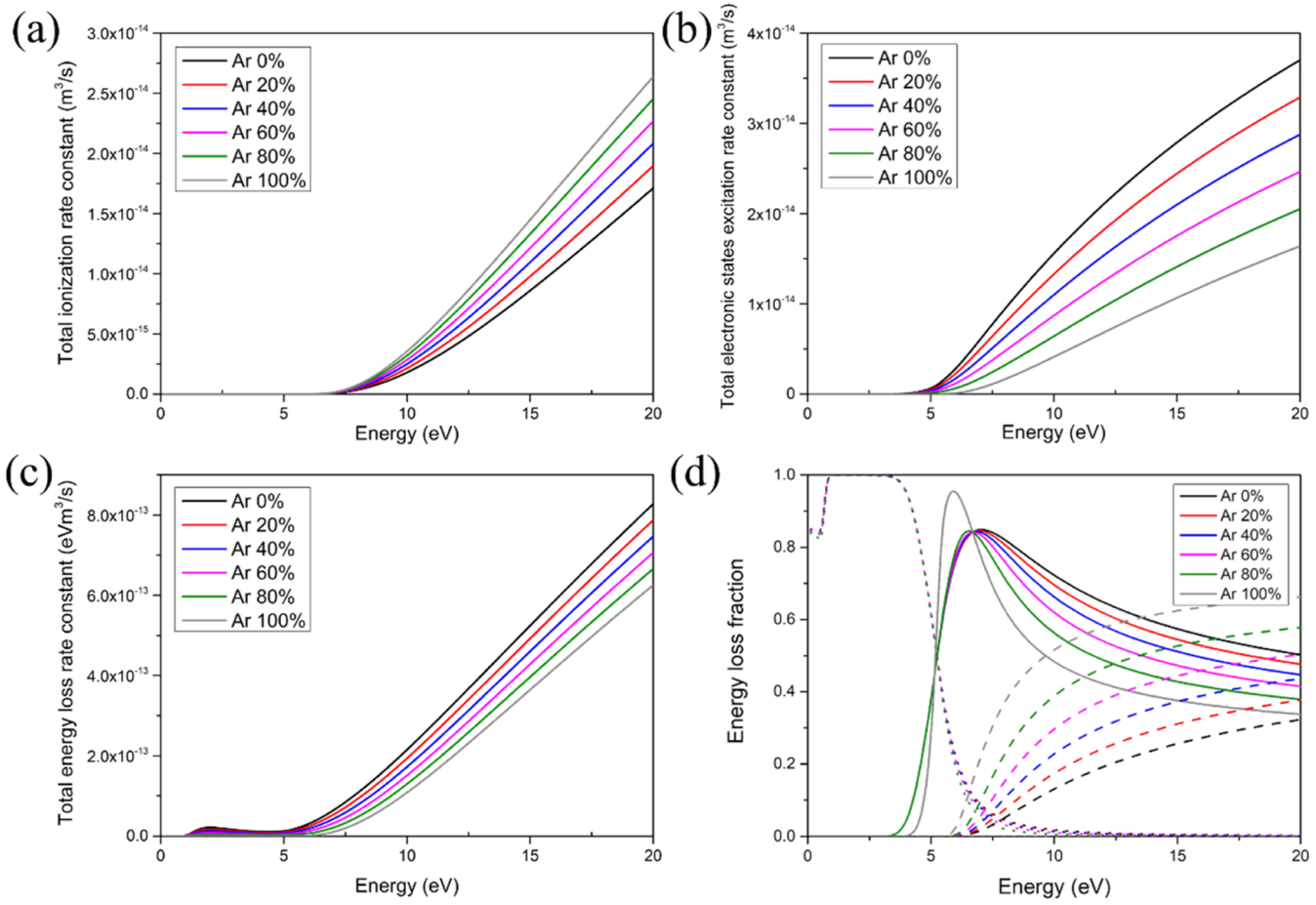

Figure 6. (a) Total ionization rate constant, (b) total electronic state excitation rate constant, (c) total energy loss rate constant, and (d) energy loss fraction of microwave-induced discharge in a mixture of nitrogen and argon. Note that the dotted and dashed lines, solid lines, and dashed lines shown in (d) represent rotational and vibrational excitation, electronic excitation, and ionization, respectively.

4. DISCUSSION

As mentioned above, the gas production and generation rate increase first and then decrease with the argon content in cracking experiments. The cracking by plasma can release more gas than pyrolysis. The results of the spectrum test indicate that the key factors are the electronic excited-state molecules, such as N_2(A, B, C), Ar(4s, 4p, 4d), and O_2(a, b), detected in the spectrum for cracking and ignition experiments. The energies of these excited-state molecules are about 1−10 eV, which are much higher than many chemical bond energies,[8] as well as the average molecular energy in the normal combustion of coal without plasma. Therefore, the molecules with an excited state in plasma cracking destroy more chemical bonds to produce more gas than that by pyrolysis. More importantly, this also means that the generation of the electronic excited state of molecules should first increase and then decrease with the argon content.

As shown in Figure 6, the generation rate of electronic excited-state molecules is $k_{Ar}N_eN_{Ar} + k_{N_2}N_eN_{N_2}$, where k_{Ar} and k_{N_2} are the reaction rate constants of electronic excited-state argon and nitrogen, respectively; and N_e, N_{Ar}, and N_{N_2} are the number densities of electron, argon, and nitrogen, respectively. Considering the low ionization degree (much less than 1%) of microwave-induced discharge under ∼1 kW microwave at atmospheric pressure,[7,24,25] the number of argon and nitrogen molecules is approximately equal to $xN_g + (1 - x)N_g$, where x is the argon content and N_g is the number of molecules of gas. Therefore, the generation rate of electronic excited-state molecules is proportional to $[xk_{Ar} + (1 - x)k_{N_2}]N_e$, abbreviated as kN_e, where k is the total electronic state excitation rate constant. As shown in Figure 6a, with an increase in argon content, the ionization rate constant increases, leading to an increase in the electron number density, N_e. Moreover, Ar has a higher scattering cross section than N_2 (shown in Figure S2), resulting in a high total ionization rate constant with increasing Ar content. However, the total electronic state excitation rate constant, k, decreases with increasing argon content, as shown Figure 6b. The energy loss rate decreases with increasing argon content, leading to an increase in the electron temperature, as shown in Figure 6c. With an increase in the argon content, the energy loss fraction of ionization increases, while the energy loss fraction of electronic state excitation decreases, as shown in Figure 6d. There is a competitive relationship between the excited and ionized states of electrons. Namely, under the same electron energy supply, the trends of the total ionization rate constant and the total electronic states excitation rate constant are opposite. Because of the increase in the ionization rate and electron energy, and the decrease of total electronic states excitation rate constant with an increase in the argon content, the generation rate of electronic states excitation molecules increases first and then decreases. Indeed, Figure 5d shows that the electron energy deposition path is affected by the energy

https://doi.org/10.1021/acsomega.3c05977
ACS Omega 2024, 9, 8947−8953

and gas composition, while the electronic energy is used for rotational or vibrational excitation, electronic excitation, and ionization processes, respectively. Therefore, there is a competitive relationship between the excited and ionized states of electrons. Namely, under the same electron energy supply, the trends of the total ionization rate constant and the total electronic states excitation rate constant are opposite. Moreover, Ar has a higher scattering cross section than N_2 (shown in Figure S2), resulting in a high total ionization rate constant with increasing Ar content.

5. CONCLUSIONS

This work investigated the microwave-induced discharge cracking and assisted ignition of anthracite. The main volatile products are CO and CO_2 in plasma cracking and pyrolysis. The gas generation rate of microwave cracking is higher than that of pyrolysis. This study advances the understanding of the cracking of low-volatile anthracite and the production of volatiles through microwave-induced discharge and can provide a reference for the ignition of low-volatile anthracite. The main conclusions are as follows:

(1) The total gas production rate, total gas production, and the amount of CO are the highest in 20% argon. This is mainly because of the increase in the number of electrons and the decrease in the electronic state excitation rate constant with an increase in argon content.
(2) The production of CO and CO_2 by plasma cracking is higher than that by pyrolysis, which indicates the cracking of polyaromatic hydrogen in anthracite by plasma. This is mainly because the energies of these excited-state molecules are much higher than many chemical bond energies of coal.
(3) The de-excitation lines of N_2(C) and Ar(4d, 4p) were detected in plasma cracking, which shows the existence of a kinetic effect on anthracite cracking by microwave-induced discharge.
(4) In the microwave-induced discharge-assisted combustion experiment, the presence of NO demonstrates that combustion was drastic, and the de-excitation lines of N_2(C) and O_2(b) demonstrate that the kinetic effect still exists in this plasma-assisted combustion experiment of anthracite.

■ ASSOCIATED CONTENT

Supporting Information

The Supporting Information is available free of charge at https://pubs.acs.org/doi/10.1021/acsomega.3c05977.

Micrographs of samples and cross-sectional data (PDF)

■ AUTHOR INFORMATION

Corresponding Author

Pengxiang Wang − *School of Energy Science and Engineering, Harbin Institute of Technology, Harbin 150001, China;* orcid.org/0000-0003-3483-6810; Email: pengxwang@qq.com

Authors

Lei Zhang − *School of Energy Science and Engineering, Harbin Institute of Technology, Harbin 150001, China*

Mingjun Liu − *School of Energy Science and Engineering, Harbin Institute of Technology, Harbin 150001, China*

Minghong Han − *School of Astronautics, Harbin Institute of Technology, Harbin 150001, China*

Yang Yu − *School of Astronautics, Harbin Institute of Technology, Harbin 150001, China*

Wei Zhou − *School of Energy Science and Engineering, Harbin Institute of Technology, Harbin 150001, China;* orcid.org/0000-0001-5126-0708

Jihui Gao − *School of Energy Science and Engineering, Harbin Institute of Technology, Harbin 150001, China;* orcid.org/0000-0003-4833-7836

Yanlin Su − *School of Energy Science and Engineering, Harbin Institute of Technology, Harbin 150001, China*

Junfeng Li − *School of Energy Science and Engineering, Harbin Institute of Technology, Harbin 150001, China*

Guangbo Zhao − *School of Energy Science and Engineering, Harbin Institute of Technology, Harbin 150001, China*

Complete contact information is available at: https://pubs.acs.org/10.1021/acsomega.3c05977

Notes

The authors declare no competing financial interest.

■ ACKNOWLEDGMENTS

The financial support from the Program of Natural Science Foundation of China (Grant No. 51876051) is acknowledged.

■ REFERENCES

(1) Rohani, V.; Takali, S.; Gérard, G.; Fabry, F.; Cauneau, F.; Fulcheri, L. A New Plasma Electro-Burner Concept for Biomass and Waste Combustion. *Waste Biomass Valorization* **2017**, *8*, 2791−2805.
(2) Peregudov, V. S. Optimization of the Process of Plasma Ignition of Coal. *High Temp.* **2009**, *47* (2), 181−186.
(3) Riaza, J.; Khatami, R.; Levendis, Y. A.; Aivarez, L.; Gil, M. V.; Pevida, C.; et al. Single particle ignition and combustion of anthracite, semi-anthracite and bituminous coals in air and simulated oxy-fuel conditions. *Combust. Flame* **2014**, *161*, 1096−1108.
(4) Messerle, V. E.; Karpenko, E. I.; Ustimenko, A. B. Plasma assisted power coal combustion in the furnace of utility boiler: Numerical modeling and full-scale test. *Fuel* **2014**, *126*, 294−300.
(5) Van Durme, J.; Dewulf, J.; Sysmans, W.; Leys, C.; Van Langenhove, H. Abatement and degradation pathways of toluene in indoor air by positive corona discharge. *Chemosphere* **2007**, *68*, 1821−1829.
(6) Van Laer, K.; Bogaerts, A. Influence of gap size and dielectric constant of the packing material on the plasma behaviour in a packed bed DBD reactor: A fluid modelling study. *Plasma Processes Polym.* **2017**, *14*, No. 1600129.
(7) Rafatov, I. R. On the Modelling of a Nonequilibrium Spherical Microwave Discharge at Atmospheric Pressure. *Contrib. Plasma Phys.* **2007**, *47* (3), 139−146.
(8) Ju, Y.; Sun, W. Plasma assisted combustion: Dynamics and chemistry. *Prog. Energy Combust. Sci.* **2015**, *48*, 21−83.
(9) Sun, J.; Wang, W.; Yue, Q.; Ma, C.; Zhang, J.; Zhao, X.; Song, Z. Review on microwave−metal discharges and their applications in energy and industrial processes. *Appl. Energy* **2016**, *175*, 141−157.
(10) Sun, J.; Wang, Q.; Wang, W.; Song, Z.; Zhao, X.; Mao, Y.; Ma, C. Novel treatment of a biomass tar model compound via microwave-metal discharges. *Fuel* **2017**, *207*, 121−125.
(11) Liu, S.; Mei, D.; Wang, L.; Tu, X. Steam reforming of toluene as biomass tar model compound in gliding arc discharge reactor. *Chem. Eng. J.* **2016**, *307*, 793−802.
(12) Hitobo, T.; Shiroki, M.; Nabesawa, H.; Asaji, T.; et al. Development of titanium micromold manufacturing technology for the microfluidic chip by plasma etching. *J. Vaccum Soc. Japan* **2017**, *60* (4), 145−147.

(13) Li, Y.; Fan, Z.; Shi, J.; Liu, Z.; Zhou, J.; Shangguan, W. Removal of Volatile Organic Compounds (VOCs) at Room Temperature Using Dielectric Barrier Discharge and Plasma-Catalysis. *Plasma Chem. Plasma Process.* **2014**, *34* (34), 801−810.
(14) Lemmens, A. K.; Rap, D. B.; Thunnissen, J. M. M.; Willemsen, B.; Rijs, A. M. Polycyclic aromatic hydrocarbon formation chemistry in a plasma jet revealed by IR-UV action spectroscopy. *Nat. Comun.* **2020**, *11*, No. 269.
(15) Jiang, B.; Wen, Y.; Li, Z.; Xia, D.; Liu, X. Theoretical Analysis on the Removal of Cyclic Volatile Organic Compounds by Non-thermal Plasma. *Water, Air, Soil Pollut.* **2018**, *229*, No. 35.
(16) Su, Y.; Zhou, W.; Li, J.; Zhang, L.; Gao, J.; Wang, P.; Qin, Y. Coke-assisted microwave ignition and combustion behaviors of anthracite in a switching atmosphere. *Fuel* **2022**, *316*, No. 123316.
(17) Su, Y.; Zhou, W.; Li, J.; Gao, J.; Wang, P.; Zhao, G.; Qin, Y. Enhanced gasification effect from discharges and the formation of centimeter-scale plasma during microwave combustion of coke. *Fuel* **2023**, *332*, No. 126058.
(18) Li, H.-P.; Ostrikov, K.; Sun, W. The energy tree: Non-equilibrium energy transfer in collision-dominated plasmas. *Phys. Rep.* **2018**, *770*−*772*, 1−45.
(19) Li, H.-Y.; Huang, P.-H.; Chao, Y.-C. Flame Enhancement by Microwave-Induced Plasma: The Role of Major Bath Gas N_2 Versus Ar. *Combust. Sci. Technol.* **2016**, *188*, 11−12.
(20) Li, J.; Zhou, W.; Su, Y.; Zhao, Y.; Qu, Z.; Xie, L.; Xue, N.; Meng, X.; Gao, J.; Sun, F.; et al. Enhancing inter-particle microwave discharge for efficient coke-CO_2 gasification. *Fuel* **2023**, *351*, No. 128817.
(21) Zhang, K.; Ding, L.; Chai, M.; Fu, Z.; Chen, J.; Hou, C.; Lv, H. Kinetic investigations of coal gasification for high-purity H2 production with carbon capture and storage potential. *J. Energy Inst.* **2023**, *111*, No. 101411.
(22) Hagelaar, G. J. M.; Pitchford, L. C. Solving the Boltzmann equation to obtain electron transport coefficients and rate coefficients for fluid models. *Plasma Sources Sci. Technol.* **2005**, *14*, 722−733.
(23) Wang, W.; Fu, L.; Sun, J.; Grimes, S.; Mao, Y.; Zhao, X.; Song, Z. Experimental Study of Microwave-Induced Discharge and Mechanism Analysis Based on Spectrum Acquisition. *IEEE Trans. Plasma Sci.* **2017**, *45* (8), 2235−2242.
(24) Yan, S.; Greenwood, A. D.; Jin, J.-M. Simulation of High-Power Microwave Air Breakdown Modeled by a Coupled Maxwell-Euler System With a Non-Maxwellian EEDF. *IEEE Trans. Antennas Prod.* **2018**, *66* (4), 1882−1893.
(25) Liu, M.; Zhang, L.; Zhou, W.; Gao, J.; Wang, P.; Zhao, G. The mechanism of microwave-induced discharge between submillimeter active coke. Plasma Source. *Plasma Sources Sci. Technol.* **2020**, *29*, No. 075015.

https://doi.org/10.1021/acsomega.3c05977
ACS Omega 2024, 9, 8947−8953